OPEN SOURCE SOFTWARE TO SIMULATE Ti:SAPPHIRE AMPLIFIERS*

D. L. Bruhwiler, B. Nash, D. T. Abell, G. Khalsa, RadiaSoft LLC, Boulder, CO, USA
J. van Tilborg, Q. Chen, C. Tóth, C. G.R. Geddes, LBNL, Berkeley, CA, USA
N. B. Goldring, STATE33 Inc., Portland, Oregon, USA

Abstract

The design of next-generation PW-scale fs laser systems, including scaling to kHz rates and development of new laser gain media for efficiency, will require parallel multiphysics simulations with realistic errors and nonlinear optimization. There is currently a lack of broadly available modeling software that self-consistently captures the required physics of gain, thermal loading and lensing, spectral shaping, and other effects required to quantitatively design such lasers [1]. We present initial work towards an integrated multiphysics capability for modeling pulse amplification in Ti:Sa lasers. All components of the software suite are open source. The Synchrotron Radiation Workshop (SRW) [2–6] is being used for physical optics, together with Python utilities. The simulations are being validated against experiments.

EXPERIMENTS

Pump-probe experiments of Ti:Sa thermal lensing have been performed at the HTU line of the BELLA Center [7], with a schematic and photo seen in Fig. 1. The 532 nm Gaussian pump beam from a kHz Revolution laser has a FWHM diameter of 1.2 mm, a FWHM pulse duration of 500 ns, and an averaged power of 19.6 W (35 mJ per pulse).

This beam pumps and heats a 1 cm diameter, 2.5 cm long Ti:Sa crystal, which has its c-axis parallel to the optical table and is water cooled. The thermal lensing effects were diagnosed with probe beams from the kHz rep rate 800 nm Coherent FrontEnd Laser System, with a FWHM pulse duration of 300 ps. The transmitted pump wavefronts were measured using a HASO wavefront sensor (WFS). A DG535 is used to control the relative delay between the pump and probe to sub-microsecond levels. Waveplates are used to tune the polarization of both pump and probe beams.

SIMULATION AND OPTICS

The software development uses operator splitting, where the laser pulse and crystal are sliced in a manner that enables robust and rapid 2D computations, leveraging the SRW code. The software is in a GitHub repository [8]. Figure 2 shows the WFS image pair, each 32x32 pixels. The intensity and phase data is used to construct real and imaginary electric fields of the longitudinally integrated wavefront, with no need to include the rapid variation in space and time. These fields are used to construct a native SRW wavefront object, which can be propagated with full physical optics. The phase distribution is essentially flat, to within measurement uncertainties.
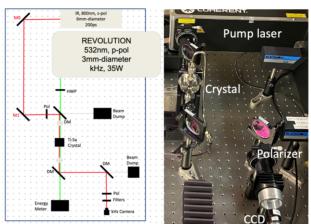

Figure 1: Design (left) and implementation (right) of the thermal lensing measurements. The pump laser deposits up to 35mJ per pulse in the Ti:Sa crystal at 1 kHz. The 800 nm, 300 ps probe pulse is synchronized with the pump. A wavefront sensor (not shown) is used to measure any effects.
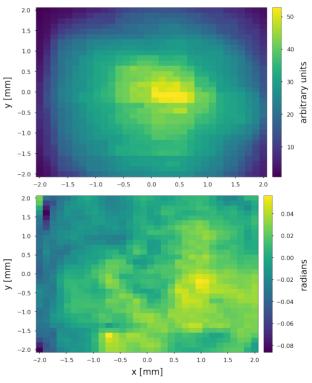

Figure 2: Wavefront sensor (WFS) measurements of a 0.8 nm probe pulse after propagating through an unpumped crystal; the intensity (upper) and phase (lower) are obtained simultaneously. This is the initial condition for SRW simulations. The low resolution is characteristic of WFS data.

MC7: Accelerator Technology

T25: Lasers

THPOTK063

2925

We propagate general 2D wavefronts via linear canonical transforms [9], using the decomposition of Pei and Huang [10] to recast a standard ABCD matrix into three, each of which SRW can use to transform the wavefront with physical optics. We are also developing a Python library for Linear Canonical Transforms which will enable wavefront propagation via more general ABCD matrices [11].

In addition, a Gaussian optics model may be applied by use of the complex beam parameter q [12]:

$$\frac{1}{q} = \frac{1}{R} - i \frac{\lambda}{\pi w^2} \quad (1)$$

with R the beam radius of curvature, λ the wavelength and w the beam size. Given an ABCD matrix for the crystal, the parameter q propagates as

$$q_f = \frac{A q_i + B}{C q_i + D} \quad (2)$$

We assume quadratic phase variation near the axis:

$$\Phi(r) = \Phi_0 - \alpha r^2 \quad (3)$$

with Φ_0 a constant phase and the phase curvature α related to the complex beam parameter via

$$\alpha = \frac{1}{2} \Re \left(\frac{1}{q} \right) \quad (4)$$

The phase above has units of length. If $\phi(r)$ is the phase in radians, $\Phi(r) = \phi(r) \frac{\lambda}{2\pi}$ with λ the laser pulse wavelength.

We can relate the phase curvature with and without the pump laser by using the ABCD matrix for a Gaussian duct:

$$M = \begin{pmatrix} \cos(\gamma L_c) & \frac{1}{n_0 \gamma} \sin(\gamma L_c) \\ -n_0 \gamma \sin(\gamma L_c) & \cos(\gamma L_c) \end{pmatrix} \quad (5)$$

with L_c the crystal length, and

$$n(r) = n_0 - \frac{1}{2} n_2 r^2 \quad \gamma^2 = \frac{n_2}{n_0}. \quad (6)$$

For a crystal with longitudinally varying values of n_0 and n_2 we multiply the matrices for each slice.

THERMAL LENSING

Figure 3 shows a comparison of thermal focusing from experiment (upper) and simulation (lower). The value of n_2 can be obtained from FEniCS [13, 14] simulations conducted with experimental parameters [15]. Although it is not done for Ti:Sa amplifiers, the probe beam in our experiments is larger transversely than the pump laser, allowing for sampling of both the pumped and unpumped regions. This results in a non-Gaussian intensity profile, because the wings are not focused. This will be included in future work.

The lower image of Fig. 3 was simulated with n_2 increased artificially by 5x, to obtain the same peak intensity (see the colorbar on the right side of each image). This discrepancy
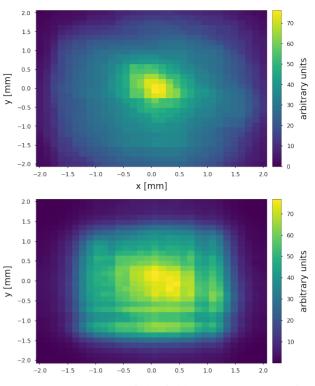

Figure 3: WFS image of the field intensity (upper) after propagation through a pumpled Ti:Sa crystal, demonstrating thermal lensing effects, to be compared with the upper image of Fig. 2. Lower image shows the field intensity of an SRW wavefront, instantiated from the data of Fig. 1 and propagated as described in the previous section.

is seen in other data as well, indicating that there is an additional source of focusing. The most likely candidate is thermal deformation of the front surface of the pumped crystal, which we plan to explore with FEniCS simulations.

We found that "focal length" inferences from WFS data depend sensitively on the specified fitting region, especially for non-Gaussian wavefronts, so it is preferable to compare wavefronts directly (simulation versus measurement). Nevertheless, comparisons of near-axis phase curvature are useful when done with care. For example, the upper image of Fig. 4 shows how one can fit a quadratic shape to the wavefront phase from the 20 or so pixels around the peak value. For the case shown in Fig. 3, near-axis phase curvatures in the data and the simulation are approximately equal. The lower image of Fig. 4 shows a 3D plot of the experimentally measured phase distribution.

AMPLIFICATION EFFECTS

We do not present results with laser amplification in this paper. Our algorithmic approach is to solve, for each cell of the 2D gridded laser pulse wavefront, the 1D Frantz-Nodvik (FN) equations [16], which describe propagation of a plane wave across gain material composed of two-level atoms:

$$\frac{\partial n}{\partial t} + c \frac{\partial n}{\partial z} = \sigma c n \Delta; \qquad \frac{\partial \Delta}{\partial t} = -\gamma \sigma c n \Delta, \quad (7)$$
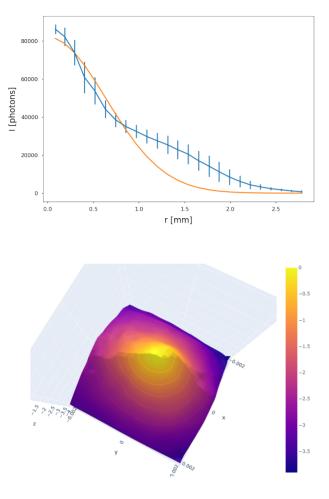
Figure 4: The upper plot corresponds to the case shown in Fig. 3, where we have fit a quadratic shape to the wavefront phase from the 20 or so pixels around the peak value. The lower image shows a 3D plot of the experimentally measured phase distribution after thermal lensing. The data also varies quadratically near the axis.

In Eq. 7, z and t denote distance along the beam axis and the time; $n(z, t)$ denotes photon number density in the medium; and $\Delta(z, t)$ denotes the "population inversion", $N_2 - N_1$, giving the difference between the number density of atoms in the excited state vs the ground state. Also, c denotes the speed of light in the medium, σ the resonance absorption cross-section, and γ a factor related to the relative degeneracy of the ground and excited states.

We use the approximate 1D solution to the FN equations, where one assumes the laser pulse intensity is a square wave. This is an adequate representation of a narrow laser pulse slice, which will yield high accuracy in the limit of many slices. The simple analytic solution also requires an assumption that the density of excited states in the crystal is independent of longitudinal position, which again is a reasonable approximation, if the crystal is represented by a sufficient number of thin slices. Convergence studies are required.

MC7: Accelerator Technology

T25: Lasers

The fundamental data structure for the Python implementation of our algorithms is the 2D wavefront object of the SRW code, which uses a 2D Cartesian mesh. Hence, we can solve the 1D FN equations in each cell of the wavefront mesh, to be done independently for each of many laser pulse slices. The approximate analytic FN solution is difficult to interpret as presented in the literature. We have a detailed derivation that will be presented in a future paper.

The simplest case is that of a square laser pulse of duration τ and a uniform photon density n_0 incident on a crystal of length L and uniform population inversion Δ_0. We define η as the total number of incident photons per unit area: $\eta = n_0 c \tau$.

$$(z, t) = \frac{n_0}{1 - [1 - \exp(-\sigma \Delta_0 z)] \exp(-\gamma \sigma \eta (t - z/c)/\tau)}. \quad (8)$$

A photon that enters at time t exits at time $t + L/c$. Hence the photon density at the exit of the crystal is given by $(z, t) = (L, t + L/c)$. The energy gain G_E is the ratio of the total number of photons exiting the crystal to the total number, η, that entered the crystal.

$$G_E = \frac{1}{\gamma \sigma \eta} \ln\{1 + \exp(\sigma \Delta_0 L)[\exp(\gamma \sigma \eta) - 1]\} \quad (9)$$

Again, this result assumes uniform incident photon density, n_0, and uniform initial population inversion, Δ_0.

One can also compute the spatial variation of the population inversion after passage of the laser pulse. For a short slice of a crystal, it is adequate to approximate the final value as an average across the slice width, yielding:

$$\Delta(z, \infty) = \Delta_0 - \frac{\gamma \eta}{L}(G_E - 1), \quad (10)$$

which is consistent with the energy gain from (9).

Given this result, one can calculate for each cell of the SRW mesh a multiplication factor (the laser gain) for the local number of photons. Because SRW is a physical optics code, it works with electric field components and not photons, but the corresponding multiplication factor is straightforward to calculate. These calculations have been implemented in Python [8].

INITIAL LESSONS LEARNED

We have described initial efforts to validate new software for propagating laser pulses through Ti:Sa crystal amplifiers for high-power chirped pulse amplification systems. The simulated laser pulses are instantiated from data (i.e., WFS image pairs). The resulting wavefronts propagate well with SRW, using the Pei-Huang expansion of the ABCD matrix.

Thermal effects due to kHz-scale laser pumping yield quadratic near-axis variation of the index of refraction, which can be captured via thermal simulations of the crystal [15]. Thermal focusing effects seen in experiments are stronger than seen in simulations, indicating that there is an additional source of focusing. The most likely candidate is thermal deformation of the front surface of the pumped crystal, which will be explored with FEniCS simulations.

REFERENCES

[1] R. Falcone *et al.*, *Brightest Light Initiative Workshop Report: the Future of Intense Ultrafast Lasers in the U.S. (March 27-29, 2019, OSA Headquarters, Washington, D.C.)* 2020, `doi:10.2172/1604161`

[2] O. Chubar, *Synchrotron Radiation Workshop (SRW)*, `https://github.com/ochubar/srw`.

[3] O. Chubar and P. Elleaume, "Accurate and efficient computation of synchrotron radiation in the near field region," in *Proceedings EPAC'98*, 1998, pp. 1177–1179.

[4] O. Chubar and R. Celestre, "Memory and CPU efficient computation of the Fresnel free-space propagator in Fourier optics simulations," *Optics Express*, vol. 27, no. 20, pp. 28 750–28 759, 2019, `doi:10.1364/OE.27.028750`

[5] M. S. Rakitin *et al.*, "Sirepo: An open-source cloud-based software interface for x-ray source and optics simulations," *Journal of Synchrotron Radiation*, vol. 25, no. 6, pp. 1877–1892, 2018, `doi:10.1107/S1600577518010986`

[6] O. Chubar, P. Elleaume, S. Kuznetsov, and A. A. Snigirev, "Physical optics computer code optimized for synchrotron radiation," in *Optical Design and Analysis Software II*, vol. 4769, 2002, pp. 145–151, `doi:10.1117/12.481182`

[7] "BELLA Center." (2022), `http://bella.lbl.gov`

[8] "The open source github repository for the `rslaser` library." (2022), `https://github.com/radiasoft/rslaser`

[9] J. Healy, M. Kutay, H. Ozaktas, and J. Sheridan, *Linear Canonical Transforms: Theory and Applications*. 2016, vol. 198, `doi:10.1007/978-1-4939-3028-9`

[10] S.-C. Pei and S.-G. Huang, "Two-dimensional nonseparable discrete linear canonical transform based on cm-cc-cm-cc decomposition," *J. Opt. Soc. Am. A*, vol. 33, no. 2, pp. 214–227, 2016, `doi:10.1364/JOSAA.33.000214`

[11] B. Nash, D. T. Abell, P. Moeller, I. V. Pogorelov, and N. B. Goldring, "Linear Canonical Transform Library for Fast Coherent X-Ray Wavefront Propagation," presented at IPAC'22, Bangkok, Thailand, Jun. 2022, paper THPOPT068, this conference.

[12] A. E. Siegman, *Lasers*. University Science Books, 1986.

[13] S. Ortiz-Laverde, C. Rengifo, M. Cobo, and M. Figueredo, "Proposal of an open-source computational toolbox for solving PDEs in the context of chemical reaction engineering using FEniCS and complementary components," *Heliyon*, vol. 7, no. 1, e05772, 2021, `doi:10.1016/j.heliyon.2020.e05772`

[14] "FEniCS." (2022), `https://fenicsproject.org/`

[15] D. T. Abell *et al.*, "Thermal modeling and benchmarking of crystalline laser amplifiers," presented at IPAC'22, Bangkok, Thailand, Jun. 2022, paper THPOTK062, this conference.

[16] L. M. Frantz and J. S. Nodvik, "Theory of pulse propagation in a laser amplifier," *J. Appl. Phys.*, vol. 34, no. 8, pp. 2346–2349, 1963, `doi:10.1063/1.1702744`